the FEBS Journal

Sodium butyrate inhibits platelet-derived growth factor-induced proliferation and migration in pulmonary artery smooth muscle cells through Akt inhibition

Silvia Cantoni[1,2,*], Margherita Galletti[1,2,*], Filippo Zambelli[1,3], Sabrina Valente[2], Francesca Ponti[1], Riccardo Tassinari[1,2], Gianandrea Pasquinelli[2], Nazzareno Galiè[2] and Carlo Ventura[1,2]

1 Laboratory of Molecular Biology and Stem Cell Engineering, National Institute of Biostructures and Biosystems, Bologna, Italy
2 Specialized Experimental and Diagnostic Medicine, University of Bologna, Italy
3 Società Italiana Studi Medicina della Riproduzione (S.I.S.Me.R.), Reproductive Medicine Unit, Bologna, Italy

Keywords
Akt; cell migration; cell proliferation; pulmonary artery smooth muscle cells; sodium butyrate

Correspondence
C. Ventura, Laboratory of Molecular Biology and Stem Cell Engineering, National Institute of Biostructures and Biosystems, Strada Maggiore 42, 40125 Bologna, Italy
Fax: +39 051340339
Tel: +39 051340339
E-mail: carlo.ventura@unibo.it, cvent@libero.it

*These authors contributed equally to this work

(Received 19 November 2012, revised 5 February 2013, accepted 4 March 2013)

doi:10.1111/febs.12227

Sodium butyrate (BU) is a molecule that acts as a histone deacetylase inhibitor. As compared with its well-known antineoplastic/antiproliferative effects, little is known about BU action on vascular cell dynamics. An imbalance of proliferation and migration in pulmonary arterial smooth muscle cells (PASMCs) is essential in the onset and progression of pulmonary arterial hypertension (PAH), a disease that is characterized by vascular lung derangement and that frequently has an unfavorable outcome. Here, we show that, in PASMCs of PAH rats, BU counteracted platelet-derived growth factor (PDGF)-induced Ki67 expression, and arrested the cell cycle, mainly at G_0/G_1. BU decreased proliferating cell nuclear antigen, c-Myc and cyclin D1 transcription and protein expression, while increasing p21 expression. BU reduced the transcription of PDGF receptor-β, and that of Ednra and Ednrb, two major receptors in PAH progression. Wound healing, migration and pulmonary artery ring assays indicated that BU inhibited PDGF-induced PASMC migration. BU strongly inhibited PDGF-induced Akt phosphorylation, an effect reversed by the phosphatase inhibitor calyculin A. BU-treated cells showed a remarkable increase in acetylated Akt, indicating an inverse relationship between the levels of acetylated Akt and phospho-Akt. These findings may provide novel perspectives on the use of histone deacetylase inhibitors in PAH.

Introduction

Pulmonary arterial hypertension (PAH) is defined as a group of diseases characterized by a progressive increase in pulmonary vascular resistance leading to right ventricular failure and premature death [1]. All types of PAH are characterized by abnormalities of pulmonary vascular biology in each compartment of the blood vessels. The lumen has a prothrombotic diathesis, and the endothelium shows excessive production of vasoconstrictors relative to vasodilators, as well as an increase in mitogenic mediators [2]. Proliferation and migration are two important features in PAH, and both smooth muscle cells and fibroblasts

Abbreviations
[^{3}H]Tmd, tritiated thymidine; AgNOR, silver-stained nucleolar organizer region; AV, annexin V; BU, sodium butyrate; histone deacetylase inhibitor; GAPDH, glyceraldehyde-3-phosphate dehydrogenase; HDAC, histone deacetylase; HPF, high-power field; MCT, monocrotaline; MTT, 3-(4,5-dimethylthiazol-2-yl)-2,5-diphenyl-tetrazolium bromide; na/nA, nucleolar area/nuclear area; PAH, pulmonary arterial hypertension; PASMC, pulmonary arterial smooth muscle cell; PCNA, proliferating cell nuclear antigen; PDGF, platelet-derived growth factor; PDGFRβ, platelet-derived growth factor receptor-β; PI3K, phosphoinositide 3-kinase; PI, propidium iodide; PP, protein phosphatase; TEM, transmission electron microscopy; TGFβR1, transforming growth factor-β receptor-1; TSA, Trichostatin-A.

contribute to 'neointima' formation, leading to vascular occlusion [3].

Within numerous signaling cascades governing pulmonary arterial smooth muscle cell (PASMC) proliferation and migration in vascular remodeling, the platelet-derived growth factor (PDGF) pathway plays a pivotal role [4]. Tyrosine kinase inhibitors such as imatinib have been shown to possess reverse remodeling potential in preclinical models of pulmonary hypertension by inducing apoptosis and blocking proliferation [5]. These observations prompt the need to focus on the development of causal treatments targeted to the normalization of the vessel structure and morphogenesis, rather than simply making use of the vasodilating action of already existing compounds. To this end, histone deacetylase (HDAC) inhibitors are known as a class of anticancer agents that are able to arrest cell proliferation and promote cell differentiation or apoptosis [6–8]. At the molecular level, they cause reactivation of epigenetically silenced genes by finely tuning histone acetylation. Furthermore, it is evident that the growth-inhibitory effect of HDAC inhibitors is reflected in the transcriptional control of several cell cycle regulators [9]. Among HDAC inhibitors, sodium butyrate (BU) is widely reported to have many cytoprotective, chemopreventive and chemotherapeutic activities, mainly through the arrest of cell proliferation, induction of apoptosis or stimulation of cell differentiation by selectively altering gene expression. Accordingly, Ranganna *et al.* showed that BU inhibited vascular smooth muscle cell proliferation by affecting the gene expression of a large number of both positive and negative growth regulators, ultimately causing growth arrest in vascular smooth muscle cells [10]. Recently, HDAC inhibitors were also found to suppress hypoxia-induced cardiopulmonary remodeling through an antiproliferative mechanism [11]. Because of their antiproliferative and antimigratory effects, HDAC inhibitors have also been widely studied in cancer and in atherosclerotic diseases, whereas their specific actions in PAH have long remained unexplored. Very recently, Zhao *et al.* reported that protein levels of HDAC1 and HDAC5 were elevated in patients with idiopathic PAH, and that HDAC inhibitors were able to mitigate the development of hypoxia-induced pulmonary hypertension in rats, and exerted antiproliferative effects on human and animal vascular cells in culture [12]. Nevertheless, the intimate molecular mechanisms underlying the HDAC inhibitor action on PAH PASMC proliferation and signaling remain to be largely unraveled. Given this lack of knowledge, this study was designed to explore whether BU modulates the proliferative action of PDGF beta homodimer in PASMCs isolated from rats with monocrotaline (MCT)-induced PAH, and whether, if this is so, HDAC inhibitors may also regulate the interplay between PDGF and Akt signaling, a major orchestrator of proliferative responses.

We provide evidence that BU acted transcriptionally in PAH PASMCs, downregulating the expression of PDGR receptor-β (PDGFRβ), as well as the gene and protein expression of major growth regulatory players. The resulting antiproliferative action was mediated by inhibition of Akt signaling by protein phosphatase (PP)1. The BU-mediated reduction in the phosphorylated state of Akt also involved a remarkable increase in its acetylation, highlighting a previously undefined role for cytosolic Akt acetylation/deacetylation in the proliferative/migratory patterning of PAH PASMCs.

Results

Cell proliferation in PASMCs isolated from healthy and MCT-treated rats

The proliferative effect of increasing concentrations of PDGF was comparatively assessed in PASMCs isolated from healthy and MCT-treated rats. As expected, both cell populations started to proliferate when fresh medium with PDGF (1, 5 or 20 $ng \cdot mL^{-1}$) was added after starvation. 3-(4,5-Dimethylthiazol-2-yl)-2,5-diphenyl-tetrazolium bromide (MTT) analysis revealed that the increase in proliferation induced by the growth factor occurred dose-dependently over a period of 120 h, and in a time-dependent fashion up to 48 h, probably because the effect of PDGF decreased after this time. After 48 and 120 h of PDGF exposure (5 and 20 $ng \cdot mL^{-1}$), proliferation was significantly more enhanced in MCT PASMCs than in cells isolated from control healthy animals (Fig. 1A), reflecting the well-known *in vivo* condition of the disease [13].

BU inhibited PDGF-induced proliferation in healthy and MCT PASMCs without affecting cell viability

In PAH PASMCs, BU dose-dependently counteracted the PDGF effect after 24 h of treatment, with cell proliferation remaining lower than that detected in cells cultured in the absence of the growth factor throughout the overall observation period. However, as 25 and 50 mM BU, as well as another HDAC inhibitor tested, 0.5 μM Trichostatin-A (TSA), depressed cell viability (Fig. 1B), the subsequent experiments were conducted in the presence of 5 mM BU, corresponding to its physiological concentration [14]. Such a concentration

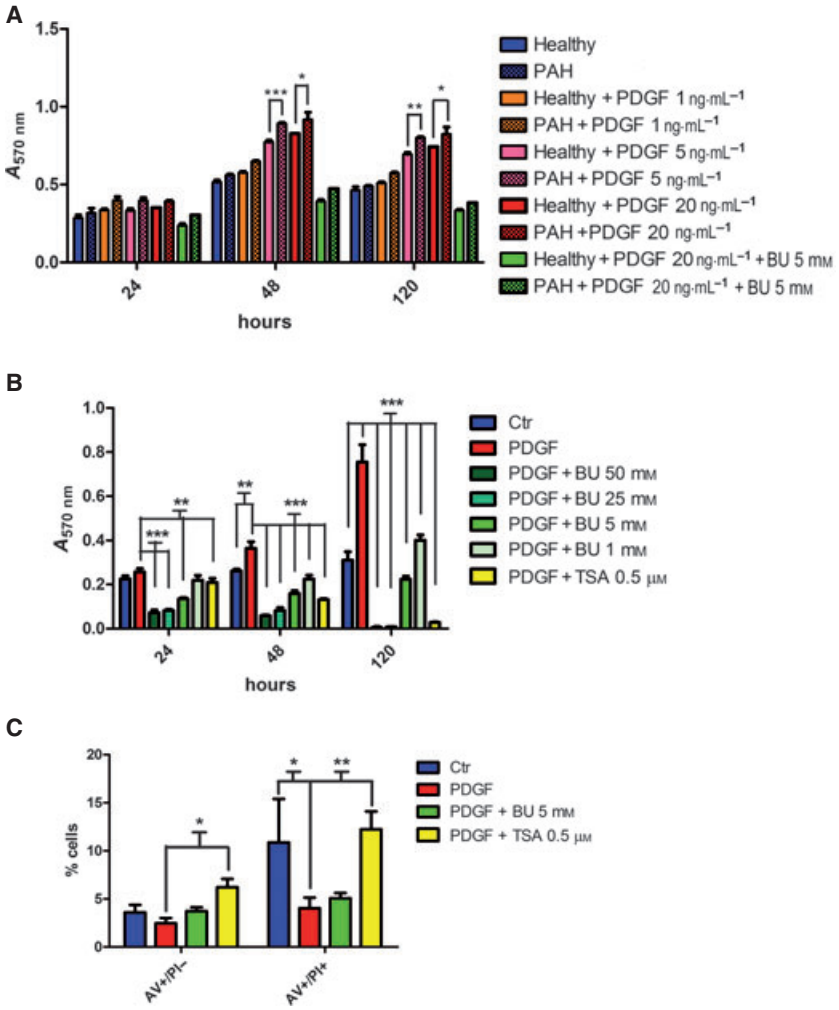

Fig. 1. Proliferation and apoptosis in PDGF-treated PASMCs. (A) MTT at 24, 48 and 120 h, using a scale concentration of PDGF ($n = 4$). Significance versus healthy cells is shown. (B) MTT at 24, 48 and 120 h, using a scale concentration of BU ($n = 5$) and 0.5 μM TSA. Significance versus stimulated cells (PDGF) is shown. (C) PI and AV double labeling. Data are expressed as percentage of living cells (AV^-/PI^-), early apoptosis (AV^+/PI^-), and late apoptosis/necrosis (AV^+/PI^+) ($n = 5$). Significance versus stimulated cells (PDGF) is shown. Statistical analysis: ANOVA with Bonferroni *post hoc* test. Significance: $*P < 0.05$, $**P < 0.01$, $***P < 0.001$. Ctr, control.

proved to be effective in inhibiting PDGF-induced proliferation in both healthy (Fig. 1A) and PAH PASMCs (Fig. 1A,B), without affecting cell viability. Moreover, the antiproliferative effect of BU was elicited to the same extent in both healthy and PAH cells (Fig. 1A).

Given the similar antiproliferative effect of BU in both cell populations, and considering the stronger proliferative response of PAH PASMCs than of healthy cells to PDGF (Fig. 1A), results from the molecular dissection of BU/PDGF patterning in these PAH cells are presented.

Annexin V (AV)–fluorescein isothiocyanate and propidium iodide (PI) staining revealed that the percentage of PAH PASMCs in early apoptosis (AV^+/PI^-) was not affected by BU (Fig. 1C). Furthermore, the percentage of cells in late apoptotis or undergoing necrotic death (AV^+/PI^+) was not altered by BU (Fig. 1C). In contrast, TSA treatment induced significant increases in both early apoptosis (AV^+/PI^-) and late apoptotis/necrotic death (AV^+/PI^+) as compared with cells exposed to PDGF alone (Fig. 1C).

BU arrested the cell cycle in PAH PASMCs

Immunofluorescence analysis showed that, following 24 h of PDGF treatment, 52 ± 7.96% of PASMCs expressed the proliferation marker Ki67, whereas the presence of 5 mM BU substantially counteracted the growth factor effect, decreasing the percentage of Ki67-positive cells (24 ± 3.84%) to a value similar to that

observed in the control group (17 ± 5.72%) (Fig. 2A, B). Similarly, cell cycle analysis (Fig. 2C) revealed that PDGF stimulation significantly decreased the percentage of quiescent cells (G_1/G_0) and increased the number of cells in the proliferative state ($S + G_2/M$), as compared with the control group. BU arrested the PASMC cell cycle mainly by blocking the transition throughout G_0/G_1 and S, thus increasing the number of quiescent cells.

Tritiated thymidine ([^{3}H]Tmd) incorporation confirmed a reduction in DNA synthesis in BU-treated cells (Fig. 2D).

BU-induced ultrastructural features of quiescent cells

Transmission electron microscopy (TEM) analysis showed that control PASMCs had the appearance of very thin, bipolar spindle-like elements, with extremely long cytoplasmic projections. This ultrastructure remained unaltered when cells were treated with a combination of BU and PDGF, whereas plump spindle-like morphology was observed in the presence of PDGF alone (Fig. 3A). Consistent with these morphological observations, the number of mitotic nuclei was similar between the control group and PASMCs concomitantly exposed to PDGF and BU, despite a remarkable increase in the mitotic figures in cells exposed to the growth factor alone (Fig. 3B,C).

Morphometric analysis of silver-stained nucleolar organizer regions (AgNORs) was used to evaluate the nucleolar/nuclear area (na/Na) ratio. Nucleoli within the PASMC nuclei showed intense dark staining without any counterstaining (Fig. 3E). Quantitative morphometric analysis revealed that the mean na/Na ratio normalized to the control was increased after PDGF treatment. In contrast, in the presence of BU, the mean na/Na ratio decreased as compared with control quiescent cells (Fig. 3D). Similar results were obtained with electron microscopy, where nucleoli were revealed through their characteristic substructure (Fig. 3F).

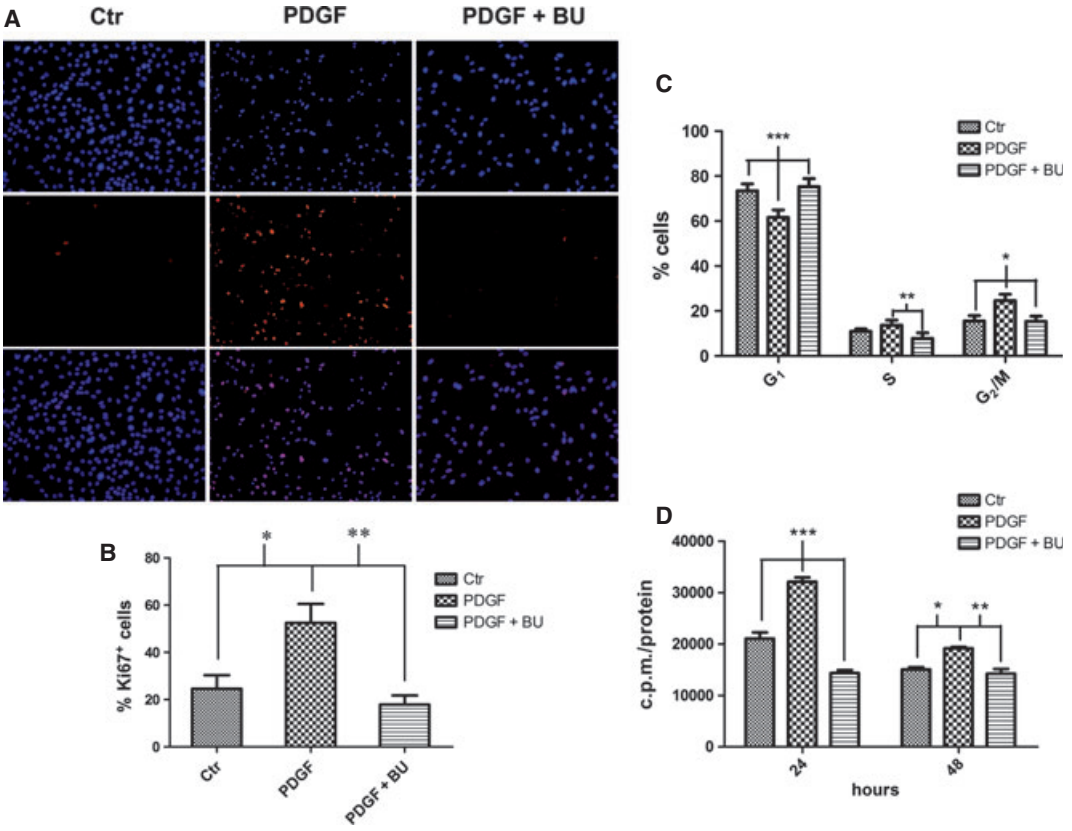

Fig. 2. BU reduced PDGF-induced proliferation of PAH PASMCs. (A) Immunofluorescence of the proliferation marker Ki67 (red); nuclei were counterstained with 4′,6-diamidino-2-phenylindole (blue); merged images are reported in the lower panels. (B) Quantification of Ki67 staining; results are expressed as percentage of positive cells normalized to the number of nuclei. (C) The percentage of cells in G_0/G_1, S and G_2/M phases of the cell cycle were determined by cytofluorimetric analysis after PI staining ($n = 3$). (D) DNA contents were estimated by [^{3}H]Tmd incorporation. Data are expressed as c.p.m. normalized to total protein content (c.p.m./protein) ($n = 5$). Statistical analysis: ANOVA with Bonferroni *post hoc* test. Significance versus stimulated cells (PDGF): $^*P < 0.05$, $^{**}P < 0.01$, $^{***}P < 0.001$. Ctr, control.

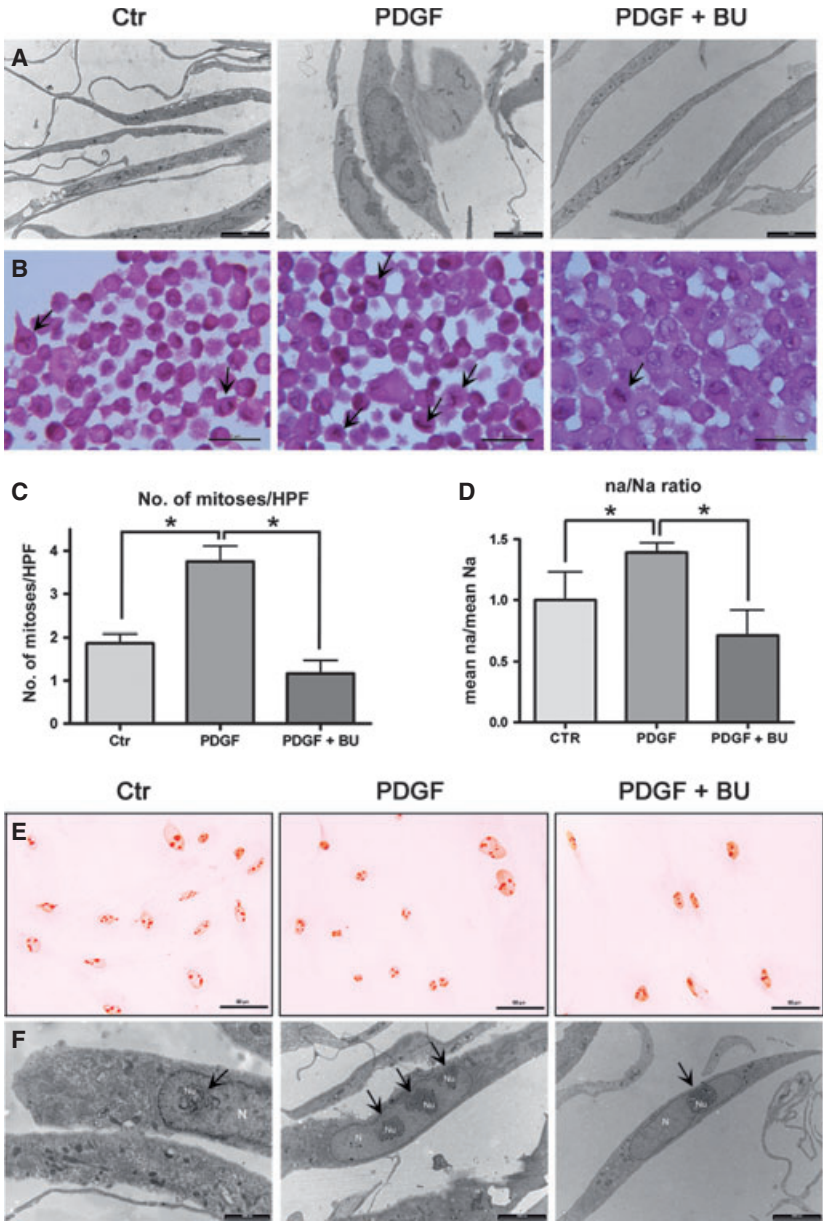

Fig. 3. Ultrastructural, histological and morphometric analysis of PASMCs. (A) TEM analysis at 24 h of treatment. Scale bars: 5 μm. (B) Representative images of pelleted cells used to count mitosis after hematoxylin and eosin staining. Original magnification: ×25. Scale bars: 50 μm. (C) Quantitative analysis of the total number of mitoses for each condition. $*P < 0.05$. (D) Results of morphometric analysis of AgNOR proteins are expressed as mean na/Na ratio normalized to control. $*P < 0.05$. (E) PASMCs selectively stained for the AgNOR proteins. Original magnification ×25. Scale bars: 50 μm. (F) Ultrastructural features of PASMC nucleoli (indicated by arrows). Nucleus (N); nucleoli (Nu). Scale bars: control (Ctr), 2 μm; PDGF and BU, 5 μm.

BU regulated PASMC proliferation at both the gene and protein expression levels

Gene expression analysis showed that BU acted at the transcriptional level in PASMC proliferation, respectively decreasing or increasing the gene expression of important positive or negative cell cycle regulators. None of these genes was affected within the first 3 h of treatment (data not shown). However, after 6 h of BU exposure, proliferating cell nuclear antigen (PCNA), c-Myc and cyclin D1 expression levels were significantly decreased as compared with exposure to PDGF alone (Fig. 4A). At the same time, the expression levels of the negative regulators p21 and

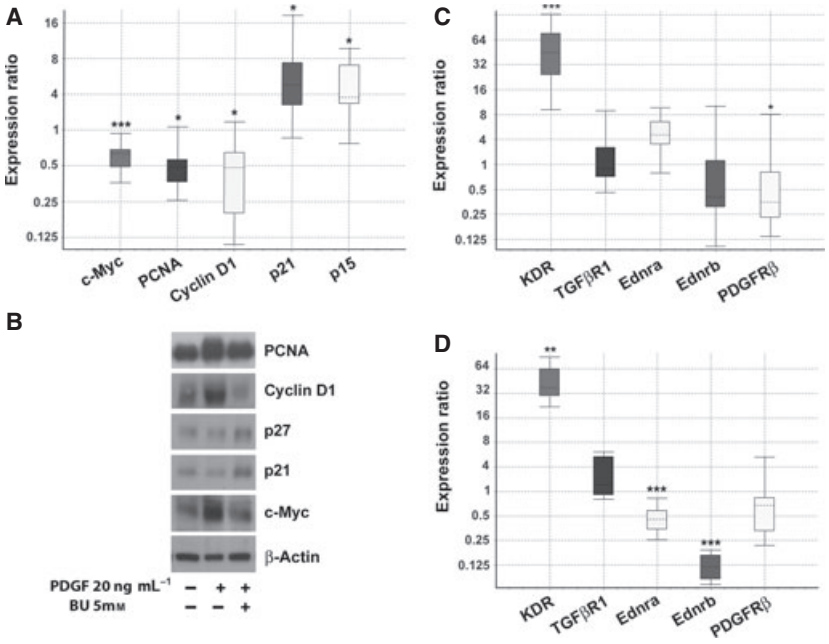

Fig. 4. BU acted at the gene and protein expression levels. (A) Gene expression analysis of positive (c-Myc, PCNA, and cyclin D1) and negative (p21 and p15) regulators after 6 h of treatment. (C, D) Gene expression analysis of the crucial signaling receptors PDGFRβ1, TGFβR1, KDR, Ednra and Ednrb after 6 h (C) and 24 h (D) of treatment. Real-time PCR data were normalized to GAPDH and β-actin housekeeping genes, and expressed as relative fold change of PDGF + BU as compared with PDGF treatment ($n = 5$). Statistical analysis: REST 2009 (Qiagen). Significance versus stimulated cells (PDGF): $*P < 0.05$, $**P < 0.01$, $***P < 0.001$. (B) Immunoblotting analysis of positive (c-Myc, cyclin D1, and PCNA) and negative (p21 and p27) regulators of the cell cycle after 8 h of treatment. The images shown are representative of five independent experiments.

p15 were significantly increased as compared with PDGF exposure (Fig. 4A). After 24 h of treatment with BU, only PCNA gene expression was still decreased (data not shown). At the protein expression level, treatment with HDAC inhibitor decreased c-Myc, cyclin D1 and PCNA expression after 8 h (Fig. 4B). At the same time, p27 expression was not affected, whereas p21 expression was increased (Fig. 4B).

BU differentially affected the gene expression of crucial signaling receptors

As early as 3 h after the start of treatment, BU significantly reduced the gene expression of PDGFRβ as compared with PDGF treatment (data not shown), the maximal transcriptional decrease being reached after 6 h (Fig. 4C). At 24 h of treatment, BU downregulated the transcription of genes encoding Ednra and Ednrb (Fig. 4D), two G-protein-coupled receptors of the ET-1 family that are deeply involved in PAH progression [15]. Conversely, BU did not affect transforming growth factor-β receptor-1 (TGFβR1) gene expression, whereas it increased the transcription of KDR, a major vascular endothelial growth factor receptor (Fig. 4C,D).

BU inhibited PDGF-induced migration

Two different migration assays were used to evaluate the effect of BU on PDGF-induced migration of PASMCs. First, we examined the effect of 5 mM BU on cell migration with a wound healing migration assay (Fig. 5A,B). Starved PASMCs were exposed to PDGF for 16 h in the absence or presence of BU. At the end of the incubation time, the wound was inflicted, and migration was monitored. At each investigated time point, the presence of BU substantially counteracted the migratory action of PDGF, even at late times (16–24 h), when cells solely exposed to the growth factor were induced to completely cover the wound area. The area of migration was calculated after 6 h (Fig. 5B) in order to reduce any effect resulting from a proliferation process. To confirm the inhibitory effect of BU on PDGF-induced migration, we performed pulmonary artery ring assays. In this model, starting from 6 days, PDGF induced progressive sprouting of

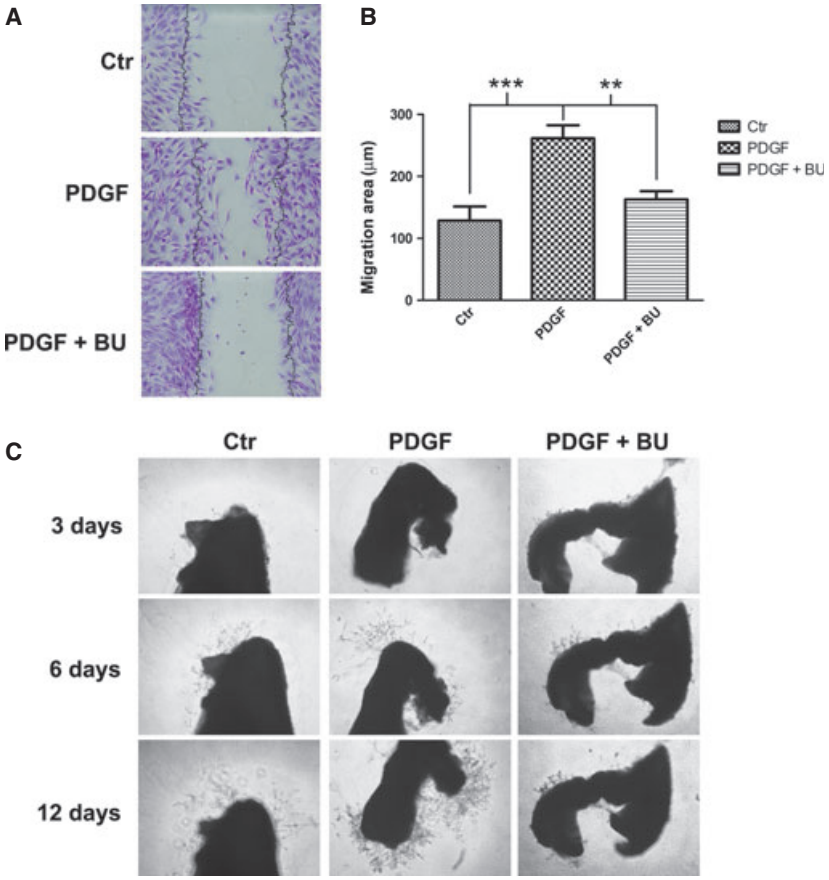

Fig. 5. BU inhibited PDGF-induced migration of PASMCs. (A) PASMCs stained with crystal violet at 6 h of migration. The interrupted line indicates time zero. (B) Quantitative results of wound healing assay ($n = 6$); the measure was obtained from the difference between the migration area after 6 h and the initial area of the wound. Statistical analysis: ANOVA with Bonferroni *post hoc* test. Significance: $^{**}P < 0.01$, $^{***}P < 0.001$. (C) Pulmonary artery rings included in semisolid medium. The images shown are representative of five independent experiments. Ctr, control.

the pulmonary artery that was completely arrested by BU throughout a period of 12 days (Fig. 5C).

BU-mediated inhibition of proliferation and migration was elicited by blocking the Akt pathway

It is well known that PDGF promotes cell proliferation by activating the Akt pathway. Interestingly, Akt phosphorylation was induced by the growth factor after 1 h of treatment, even in the presence of BU and TSA (Fig. 6A). However, after 7 h of treatment in the presence of the HDAC inhibitors, the phosphorylation of Akt at Ser473 was strongly reduced, and this effect was maintained for up to 24 h (Fig. 6A). The phosphoinositide 3-kinase (PI3K) inhibitor LY294002 completely suppressed Akt activation, and consequently counteracted the stimulatory effects of PDGF on proliferation (Fig. 6B) and migration (Fig. 6C). Conversely, no additive effect of BU and LY294002 was observed.

BU and PDGF finely tuned Akt acetylation and phosphorylation

We investigated whether BU may have inhibited PDGF-induced Akt activation through a deacetylase inhibitory action.

In agreement with previous studies [16], Akt was found to be endogenously acetylated. Whereas basal acetylation was not affected by PDGF, protein expression analysis revealed that, after 7 h, a time point at which BU elicited significant downregulation of phosphorylated Akt, BU-treated cells also showed a remarkable increase in the level of acetylated Akt (Fig. 7A). Time course analysis also revealed that

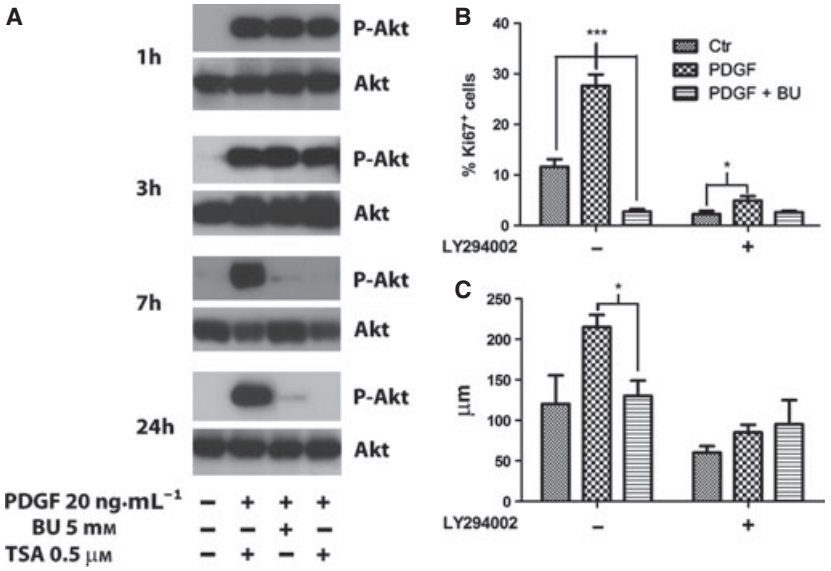

Fig. 6. BU affected the Akt pathway. (A) Time course of phospho-Akt(Ser473) (P-Akt), and total Akt, in PASMCs treated with PDGF in the presence or absence of BU or TSA; untreated cells were used as a control. Representative blots from nine independent experiments are shown. (B) Quantification of Ki67 staining after 24 h in the presence or absence of the PI3K inhibitor LY294002. Results are expressed as percentage of positive cells normalized to the number of nuclei. (C) Quantification of migration area after 6 h of migration in the presence or absence of the PI3K inhibitor LY294002. Statistical analysis for (B) and (C): ANOVA with Bonferroni *post hoc* test. Significance: $*P < 0.05$, $**P < 0.01$, $***P < 0.001$.

BU-mediated acetylation was already evident at 1 h, a time point at which Akt was still phosphorylated (Fig. 7B).

BU-mediated inhibition of Akt signaling was dependent on calyculin A-sensitive protein phosphatase activity

We next investigated whether the ability of BU to downregulate Akt phosphorylation may result from facilitation of Akt dephosphorylation by a mechanism involving PPs. To this end, we used two well-known inhibitors with distinct specificities for phosphatases: okadaic acid, which is selective for PP2A at low concentrations ($\leq$ 100 nM) [17,18], and calyculin A, which does not discriminate between PP1 and PP2A [19].

Calyculin A restored Akt phosphorylation in BU-treated cells at 7 h (Fig. 7C), whereas okadaic acid was ineffective, suggesting preferential involvement of PP1.

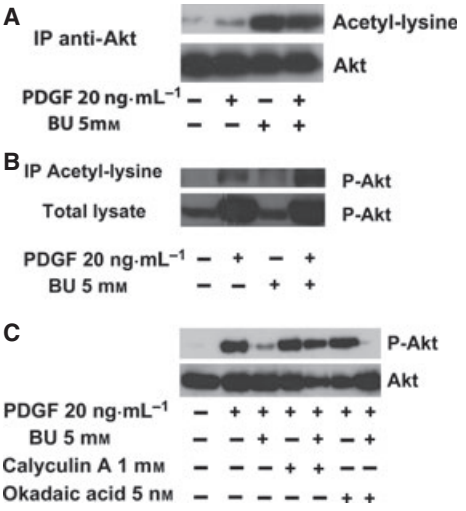

Fig. 7. BU acts through phosphatase activity. (A) Akt immunoprecipitation (IP) after 7 h of treatment with PDGF and BU; immunoblotting analysis of acetyl-lysine and Akt. (B) Comparison between the phospho-Akt(Ser473) level before (Total lysate) and after immunoprecipitation with antibody against acetyl-lysine in cells at 1 h of treatment with PDGF and BU. Representative blots from five independent experiments are shown. (C) Immunoblotting for phospho-Akt(Ser473) and total Akt after 7 h of treatment. Calyculin A and okadaic acid were added 1 h before the treatment to inhibit the phosphatase activity. The blots are representative of six independent experiments.

Discussion

Despite significant advances in the elucidation of the genetic basis for some patients, and despite progress in PAH therapy, the prognosis remains poor. The current treatment strategy, optimized in recent guidelines [20],

remains inadequate. In fact, the mortality rate continues to be high, and the functional and hemodynamic impairments are still extensive in many patients. Prior to the advent of modern therapies, the life-expectancy for adults with idiopathic PAH was 3 years from diagnosis; for children, it was 10 months [21]. The specific drugs approved for PAH are able to slow the progression of the disease, but cannot be considered to be a cure for the majority of patients [1].

Within this context, the development of treatments that may afford reverse remodeling of the vascular architecture and biology in PAH would have relevant biomedical implications. HDAC inhibitors are recognized as being promising for handling cell growth and differentiation. Nevertheless, apart from their use in cancer patients with both solid and liquid tumors, the potential exploitation of HDAC inhibitors in complex vascular diseases such as PAH has long remained elusive, and has started only very recently [11,12].

Here, we provided evidence that BU was able to control, at both the gene and protein expression levels, multiple positive and negative regulators of proliferation in PASMCs isolated from PAH rats.

Inhibition of PASMC proliferation in response to PDGF could be achieved at physiological BU concentrations that did not impair cell viability. It is noteworthy that BU was able to downregulate the gene expression of PDGFRβ and the transcription of Ednra and Ednrb, as well as PASMC migration and PDGF-induced vessel sprouting from the pulmonary artery, of PAH animals. These findings further support the hypothesis that the action of this HDAC inhibitor occurs at multiple interconnected levels of the molecular processess that impact on PASMC biology and PAH progression.

BU-mediated inhibition of PDGF-induced proliferation and migration was associated with a remarkable reduction in Akt phosphorylation after 7 h, an effect that was also achieved in the presence of TSA. These inhibitory effects were mimicked by the PI3K inhibitor LY294002, with no additive effect of BU, indicating that the antiproliferative/antimigratory action of BU was mediated by Akt dephosphorylation. The ability of the phosphatase inhibitor calyculin A to rescue Akt phosphorylation in the presence of BU and PDGF strongly suggests that phosphatase-mediated dephosphorylation of Akt may be a major underlying mechanism of HDAC inhibitor action.

Failure to restore Akt phosphorylation by okadaic acid, which is selective for PP2A at low concentrations [17,18], suggests major involvement of PP1 as compared with PP2A.

Further insights into the mechanism(s) regulating the BU-mediated phospho-Akt–phosphatase interplay can be obtained from the BU effect on Akt acetylation. Our data show that BU enhanced the level of acetylated Akt, concomitantly with phosphatase inhibitor-relievable dephosphorylation of the kinase. On the one hand, these observations raise the issue of investigating which histone acetyltransferase(s), or HDAC–-acetyltransferase interplay, may be responsible for the fine-tuning of Akt acetylation. On the other hand, the BU effect suggests that HDAC inhibition may have blocked HDAC–phosphatase interaction(s), thus promoting the release of phosphatase and its subsequent association with Akt, its acetylated form being more prone to phosphatase binding. Such a hypothesis is consistent with previous observations showing that HDAC inhibitors can disrupt the interactions of HDAC1 and HDAC6 with PP1 in human glioblastoma cells, resulting in the formation of a PP1–Akt complex and inhibition of kinase activity [22], and that Akt deacetylation promotes its phosphorylation and activation [16].

Although HDAC inhibitors are well known to induce chromatin plasticity and remodeling [23], acetylation of nonhistone proteins has been demonstrated to modulate protein functions by altering their stability, cellular localization, and protein–nucleotide/protein–protein interactions. Well-characterized targets of nonhistone acetylation include important cellular factors such as p53, nuclear factor-κB, p65, CREB-binding protein, p300, STAT3, tubulin, positive cofactor 4, GATA factors, nuclear receptors, c-Myc, hypoxia-inducible factor-1α, FoxO1, heat-shock protein-90, high-mobility group factors, E2F, MyoD, Bcr–Abl, the FLT3 kinase, and c-Raf kinase [24–26].

Our results indicate an intriguing interplay between HDACs, PP(s), and Akt acetylation/deacetylation. In this respect, acetylation and deacetylation of histones and nonhistone proteins increasingly appear to be regulated through multifaceted interrelated networks and epigenetic modification, the overall plan remaining mostly enigmatic [27] and still awaiting further clarification. Although additional studies are required to dissect the intimate mechanism(s) of the effects of HDAC inhibitors on Akt dynamics and the patterning of other nonhistone proteins, the present findings on the action of BU highlight a new role for an old molecule: its ability to behave as a fine-tuner of a crucial protein kinase involved in cell survival, proliferation, and memory. From such a viewpoint, BU can also be conceived as a multiple-target molecule, paving the way to novel perspective(s) in the clinical use of HDAC inhibitors in PAH.

Experimental procedures

Ethics statement

Animal use was approved by the Bioethics Committee of the University of Bologna, in compliance with Directive 2010/63/EU of the European Parliament. Animals received food and water *ad libitum*, and were housed under controlled conditions of light and temperature (23–25 °C).

Cell isolation and culture conditions

Adult male Sprague-Dawley rats (body weight of 200–250 g; Harlan Laboratories, Indianapolis, IN, USA) were subjected to a subcutaneous injection of 60 $mg \cdot kg^{-1}$ MCT (Sigma-Aldrich, Indianapolis, IN, USA); saline was used for untreated rats (sham) [13]. MCT was dissolved in 1 M HCl, and 1 M NaOH was added to neutralize the solution. After 28 days, all rats were anesthetized in a CO_2/O_2 mixture, and subsequently killed by cervical dislocation. Intrapulmonary arteries were isolated and cleaned of connective tissue under a stereoscopic microscope. The isolation of PASMCs from both healthy and PAH animals was performed with a modification of a previously described method [28]. The tissue was digested at 37 °C for 20 min in DMEM containing 250 $U \cdot mL^{-1}$ collagenase type I (Sigma-Aldrich). Fetal bovine serum (10%) was added to stop the reaction, and the digested pieces were placed into Petri dishes containing fresh complete medium and allowed to rest for 1 week.

Cells were cultured in complete medium consisting of high-glucose DMEM supplemented with 10% fetal bovine serum, 100 $U \cdot mL^{-1}$ penicillin, 100 $\mu g \cdot mL^{-1}$ streptomycin and 4 mM L-glutamine (all reagents from Lonza, Basel, Switzerland) at 37 °C in a humidified atmosphere of 5% CO_2.

For all experiments, PASMCs were starved on the day after seeding with medium containing a lower percentage of serum (0.5% fetal bovine serum). After 24 h, cells were induced to proliferate and migrate by replacing starvation medium with fresh medium containing 20 $ng \cdot mL^{-1}$ PDGF beta homodimer (PeProtech, Rocky Hill, NJ, USA). BU and TSA were added concurrently with the growth factor, and the inhibitors, such as 25 μM LY294002, 1 μM calyculin A, and 5 nM okadaic acid (all from Sigma-Aldrich), were administered 1 h before the treatment. PASMCs from the third to the fourth passages were used for all studies. All experiments were repeated at least five times, unless otherwise mentioned.

Cell proliferation and viability

Cell proliferation was evaluated with the MTT-based Cell Growth Determination Kit, according to the manufacturer's instructions (Sigma-Aldrich). Briefly, MTT solution was added to each well at the end of treatment and incubated for 2 h. The converted dye, insoluble purple formazan, was solubilized overnight by adding 10% SDS in a 10 mM HCl solution [29] directly to the well. Data were collected at 570 nm with a multiwell plate reader (Dynex Technology, Chantilly, VA, USA).

For cell death detection, double labeling with PI and AV was carried out with an AV-Fluos staining kit, according to the manufacturer's instructions (BD, San Diego, CA, USA). At least 10 000 events were recorded with the aid of FACSAria (BD). After the appropriate markings for the negative and positive populations had been set, the percentages of AV^-/PI^- (living cells), AV^+/PI^- (early apoptosis) and AV^+/PI^+ (late apoptosis, necrosis) staining were determined.

Immunofluorescence

PASMCs were seeded (5000 cells per cm^2), starved, and treated with molecules in low-serum medium. After 24 h, cells were washed with $NaCl/P_i$ and fixed in methanol for 10 min. Permeabilization and saturation were performed with 0.1% Triton for 15 min and 5% BSA (Sigma-Aldrich) in $NaCl/P_iP$, respectively, for 1 h. $NaCl/P_i$ added with 0.05% Tween-20 (Sigma-Aldrich) was used for washes. Primary monoclonal mouse antibody for Ki67 (Novocast, El Carmen, Mexico) and the secondary antibody AlexaFluor555-conjugated goat anti-mouse IgG (Invitrogen, Carlsbad, CA, USA) were suspended in 1% BSA and incubated at 37 °C for 1 h. Nuclei were labeled with 4′,6-diamidino-2-phenylindole (10 $ng \cdot mL^{-1}$) for 15 min.

Cell cycle and DNA content

The cell cycle distribution was determined after PI staining; the samples were prepared with a two-step method reported elsewhere [30]. Briefly, cells were centrifuged for 5 min at 800 ***g***, and 2×10^6 cells were resuspended in 1 mL of solution I (584 $mg \cdot L^{-1}$ NaCl, 1139 $mg \cdot L^{-1}$ sodium citrate, 10 $mg \cdot L^{-1}$ RNase, and 0.3 $mL \cdot L^{-1}$ Nonidet P-40). After 1 h on ice, 1 mL of solution II (15 $g \cdot L^{-1}$ citric acid, 85 $g \cdot L^{-1}$ sucrose, and 50 $mg \cdot L^{-1}$ PI) was added, and the samples were briefly vortexed. PI fluorescence forward scatter and side scatter of cell suspensions were used to assess the cell cycle distribution of cells (10 000 events) by flow cytometry.

To evaluate the DNA content of cells, incorporation of [^{3}H]Tmd was performed with a modification of a previously described method [31]. Briefly, the [^{3}H]Tmd (1 $\mu Ci \cdot mL^{-1}$) was added during the last 4 h of the incubation time (24 and 48 h). The acid-precipitable fraction, obtained by the use of 10% trichloroacetic acid, was dissolved in 0.3 mL of 0.5 M NaOH and neutralized with 30 μL of 5 M HCl (all from Sigma-Aldrich). Liquid scintillation ULTIMA Gold uLLT (PerkinElmer, Waltham, MA, USA) was added, and the radioactivity was measured (5 min per sample) with a Packard Tri-Carb 2100TR scintillation counter. The radioactivity of the samples was expressed as counts per minute (c.p.m.), and normalized to total protein content.

Gene expression analysis

Total RNA was isolated with an RNeasy Micro Kit (Qiagen, Düsseldorf, Germany), according to the manufacturer's instructions. For RT-PCR, cDNA was synthesized in a 20-μL reaction volume with 1 μg of total RNA and SuperScript III RT (Invitrogen). To assess the indicated genes, 0.2 μg of cDNA was used for real-time RT-PCR performed with a Lightcycler system (Roche Diagnostics, Mannheim, Germany) and with the SYBR Green fast start kit (Lightcycler FastStart DNA MasterPLUS SYBR Green I). Qiagen quantitect primers were used in real-time RT-PCR: cdkn2b (p15), kdr, tgfbr1, actb, gapdh, pcna, ednra, pdgfrb, ednrb, myc, cdkn1a (p21), and cdkn1b (p27). For each primer, a melting curve analysis was performed, and real-time PCR efficiency was calculated. Data were normalized by using glyceraldehyde-3-phosphate dehydrogenase (GAPDH) and β-actin as an index of cDNA content after reverse transcription. Results were analyzed and related plots were created with Relative Expression Software Tool (REST 2009 V2.0.13; Qiagen) [32].

SDS/PAGE and western blotting

Protein samples were prepared and immunoblots were analyzed as previously described [33]. Briefly, cells were lysed with M-PER extraction buffer supplemented with 1 mM phenylmethanesulfonyl fluoride, protease, and phosphatase inhibitor cocktail (Sigma-Aldrich). Lysates were subjected to SDS/PAGE and transferred to polyvinylidene membranes. After blocking, the membranes were probed overnight at +4 °C with primary antibodies. Rabbit anti-cMyc, rabbit anti-Akt, rabbit anti-phospho-Akt(Ser473) mouse anti-acetyl-lysine (all from Cell Signaling, Danvers, MA, USA), mouse anti-actin, mouse anti-cyclin D1 (both from BD), mouse anti-p27, rabbit anti-p21, and mouse anti-PCNA (all from Santa Cruz Biotechnology Inc., Santa Cruz, CA, USA). The membranes were then incubated for 1 h at room temperature with secondary antibodies conjugated to horseradish peroxidase: goat anti-rabbit IgG (Cell Signaling) or goat anti-mouse IgG (BD). Bound antibodies were detected with the use of Immobilon Western HRP Chemiluminescent Substrates (Millipore, Billerica, MA, USA), and quantified by densitometry. The intensities of phosphoprotein or protein bands were normalized to that of the corresponding total protein, or housekeeping protein, as indicated in the figures and legends.

Electron microscopy

The ultrastructural features of PASMCs were investigated by TEM. To preserve the natural morphology, cells were immediately washed and fixed in Karnowsky fixative (2% glutaraldeyde and 4% formaldeyde in 0.1 M phosphate buffer) directly in the culture plate for 20 min at room temperature. After mechanical removal, the cells were pelleted, fixed for a further 24 h with the same fixative at 4 °C, and processed for TEM analysis. Samples were rinsed in $NaCl/P_i$, postfixed in 1% buffered osmium tetroxide for 1 h at room temperature, dehydrated through graded ethanol, and embedded in Araldite resin. Serial semithin sections were stained with Toluidine blue. Ultrathin sections were counterstained with uranyl acetate and lead citrate, and observed in a Philips 400T (FEI Company, Milan, Italy) transmission electron microscope.

Mitosis analysis

For conventional histological analysis, pelleted cells were fixed in 10% buffered formalin and embedded in paraffin; 4-μm-thick sections were stained with hematoxylin and eosin, and viewed in a light microscope with Image-Pro Plus 6 (Media Cybernetics, Silver Spring, MD, USA). Images were digitalized through a video camera (JVC 3CCD video camera, KY-F55B; Yokohama, Japan) connected to a Leitz Diaplan light microscope (Wetzlar, Germany). Each sample was entirely digitized with a ×40 objective [final magnification ×400 = high-power field (HPF)]. The mitotic index was calculated by counting the number of mitoses per HPF.

Nucleolar organizer region silver staining and morphometric analysis

AgNOR staining and quantification were carried out to evaluate proteins associated with the nucleolar organizer regions. Cells seeded on glass slides were fixed in 2% paraformaldehyde in $NaCl/P_i$ supplemented with 1% Triton X-100. After being washed in distilled water, samples were stained with silver for 15 min at 37 °C in the dark with a solution of one volume of 2% gelatin in 1% aqueous formic acid, and two volumes of 50% silver nitrate. After being washed, cells were finally dehydrated and mounted in a synthetic medium with no counterstaining. AgNOR analysis was carried out with IMAGE-PRO PLUS, as previously reported [34]. For each experimental condition, AgNOR intensely stained nucleolar and nuclear areas of at least 60 nuclei were measured, and the results were expressed as mean na/Na ratio normalized to control.

Wound healing assay

For scratch wound assays, confluent cells were starved and stimulated with PDGF in the absence or presence of BU. Untreated cells were used as a control. After 16 h, cell layers were wounded with a 200-μL micropipette tip, the floating cells were washed away with starvation medium, and wound closure was monitored by phase microscopy for 24 h. To exclude the proliferation effect, the time point utilized for measurement of migration was 6 h. At this

time, cells were fixed with methanol for 10 min and stained with 0.1% crystal violet solution in 25% methanol for 30 min. The area of migration was determined for quantitative assessment with NIS-ELEMENTS D3.2 (Nikon, Tokyo, Japan) software, and compared with the wound area at time zero.

Pulmonary artery ring assay

Pulmonary arteries were removed from rats receiving MCT (60 mg·kg^{-1}) as described above, and immediately transferred to a 50-mL tube containing 40 mL of ice-cold, serum-free DMEM. The fibroadipose tissue was carefully removed, and artery rings were sectioned (1 mm), and rinsed extensively in three consecutive washes of DMEM. The rings were embedded in 0.3 mL of Cultrex BME (Trevigen, Gaithersburg, MD, USA), and the 48-well plates were incubated at 37 °C for 30 min to harden the semisolid medium. Then, 0.3 mL of treatment medium was added to each well, and the cultures were kept at 37 °C in a humidified environment, and fed every 3 days. Time zero, 3-day, 6-day and 10-day cultures were photographed with an inverted optical microscope equipped with a digital sight camera (Nikon).

Immunoprecipitation assay

For the immunoprecipitation analysis, cells were dissolved in M-PER extraction buffer supplemented with 1 mM phenylmethanesulfonyl fluoride, protease, and phosphatase inhibitors (Sigma). Cell extracts were centrifuged at 10 000 ***g*** for 10 min at 4 °C, and supernatants were incubated for 1 h with antibody against Akt or acetyl-lysine (Cell Signaling) and immunoprecipitated overnight at 4 °C with protein A/G–Agarose (Santa Cruz), according to the manufacturer's instructions. The beads were then isolated by centrifugation (1000 ***g*** for 5 min at 4 °C), and washed five times with M-PER buffer.

Samples were eluted in 2× loading buffer and boiled for 5 min to dissociate the immunocomplexes from the beads. Immunoprecipitates were separated by SDS/PAGE followed by immunoblotting. The blots were probed with antibodies against total Akt, phospho-Akt, and acetyl-lysine.

Statistical analysis

Significant differences among various groups were determined by ANOVA followed by an appropriate *post hoc* test, or with a two-tailed, unpaired Student's *t*-test. Values were expressed as mean ± standard error of the mean from three to nine independent experiments. Differences at $P < 0.05$ and $P < 0.01$ were considered to be statistically significant and extremely significant, respectively.

Acknowledgements

This research was supported by: Ministero della Salute, Italy, Ricerca Finalizzata – Progetti Cellule Staminali 2008 (C. Ventura); Fondazione Fornasini, Poggio Renatico, Italy (C. Ventura); Fondazione Cardinale Giacomo Lercaro, Bologna, Italy (C. Ventura); and Tavola Valdese, Rome, Italy (C. Ventura).

References

1 Galiè N, Palazzini M & Manes A (2010) Pulmonary arterial hypertension: from the kingdom of the near-dead to multiple clinical trial meta-analyses. *Eur Heart J* **31**, 2080–2086.
2 Sakao S & Tatsumi K (2011) Vascular remodeling in pulmonary arterial hypertension: multiple cancer-like pathways and possible treatment modalities. *Int J Cardiol* **147**, 4–12.
3 Sakao S, Tatsumi K & Voelkel NF (2010) Reversible or irreversible remodeling in pulmonary arterial hypertension. *Am J Respir Cell Mol Biol* **43**, 629–634.
4 Perros F, Montani D, Dorfmüller P, Durand-Gasselin I, Tcherakian C, Le Pavec J, Mazmanian M, Fadel E, Mussot S, Mercier O *et al.* (2008) Platelet-derived growth factor expression and function in idiopathic pulmonary arterial hypertension. *Am J Respir Crit Care Med* **178**, 81–88.
5 Grimminger F & Schermuly RT (2010) PDGF receptor and its antagonists: role in treatment of PAH. *Adv Exp Med Biol* **661**, 435–446.
6 Fotheringham S, Epping MT, Stimson L, Khan O, Wood V, Pezzella F, Bernards R & La Thangue NB (2009) Genome-wide loss-of-function screen reveals an important role for the proteasome in HDAC inhibitor-induced apoptosis. *Cancer Cell* **15**, 57–66.
7 Minucci S & Pelicci PG (2006) Histone deacetylase inhibitors and the promise of epigenetic (and more) treatments for cancer. *Nat Rev Cancer* **6**, 38–51.
8 Qian DZ, Kato Y, Shabbeer S, Wei Y, Verheul HM, Salumbides B, Sanni T, Atadja P & Pili R (2006) Targeting tumor angiogenesis with histone deacetylase inhibitors: the hydroxamic acid derivative LBH589. *Clin Cancer Res* **12**, 634–642.
9 Ocker M & Schneider-Stock R (2007) Histone deacetylase inhibitors: signalling towards p21cip1/waf1. *Int J Biochem Cell Biol* **39**, 1367–1374.
10 Ranganna K, Yousefipour Z, Yatsu FM, Milton SG & Hayes BE (2003) Gene expression profile of butyrate-inhibited vascular smooth muscle cell proliferation. *Mol Cell Biochem* **254**, 21–36.
11 Cavasin MA, Demos-Davies K, Horn TR, Walker LA, Lemon DD, Birdsey N, Weiser-Evans MC, Harral J, Irwin DC, Anwar A *et al.* (2012) Selective class I

histone deacetylase inhibition suppresses hypoxia-induced cardiopulmonary remodeling through an antiproliferative mechanism. *Circ Res* **110**, 739–748.
12 Zhao L, Chen CN, Hajji N, Oliver E, Cotroneo E, Wharton J, Wang D, Li M, McKinsey TA, Stenmark KR *et al.* (2012) Histone deacetylation inhibition in pulmonary hypertension: therapeutic potential of valproic acid and suberoylanilide hydroxamic acid. *Circulation* **126**, 455–467.
13 Schermuly RT, Dony E, Ghofrani HA, Pullamsetti S, Savai R, Roth M, Sydykov A, Lai YJ, Weissmann N, Seeger W *et al.* (2005) Reversal of experimental pulmonary hypertension by PDGF inhibition. *J Clin Invest* **115**, 2811–2821.
14 Burger-van Paassen N, Vincent A, Puiman PJ, van der Sluis M, Bouma J, Boehm G, van Goudoever JB, van Seuningen I & Renes IB (2009) The regulation of intestinal mucin MUC2 expression by short-chain fatty acids: implications for epithelial protection. *Biochem J* **420**, 211–219.
15 Davie N, Haleen SJ, Upton PD, Polak JM, Yacoub MH, Morrell NW & Wharton J (2002) ET(A) and ET (B) receptors modulate the proliferation of human pulmonary artery smooth muscle cells. *Am J Respir Crit Care Med* **165**, 398–405.
16 Sundaresan NR, Pillai VB, Wolfgeher D, Samant S, Vasudevan P, Parekh V, Raghuraman H, Cunningham JM, Gupta M & Gupta MP (2011) The deacetylase SIRT1 promotes membrane localization and activation of Akt and PDK1 during tumorigenesis and cardiac hypertrophy. *Sci Signal* **4**, ra46.
17 Connor JH, Kleeman T, Barik S, Honkanen RE & Shenolikar S (1999) Importance of the beta12–beta13 loop in protein phosphatase-1 catalytic subunit for inhibition by toxins and mammalian protein inhibitors. *J Biol Chem* **274**, 22366–22372.
18 Gupta V, Ogawa AK, Du X, Houk KN & Armstrong RW (1997) A model for binding of structurally diverse natural product inhibitors of protein phosphatases PP1 and PP2A. *J Med Chem* **40**, 3199–3206.
19 Resjö S, Oknianska A, Zolnierowicz S, Manganiello V & Degerman E (1999) Phosphorylation and activation of phosphodiesterase type 3B (PDE3B) in adipocytes in response to serine/threonine phosphatase inhibitors: deactivation of PDE3B in vitro by protein phosphatase type 2A. *Biochem J* **341** (Pt 3), 839–845.
20 Galiè N, Hoeper MM, Humbert M, Torbicki A, Vachiery JL, Barbera JA, Beghetti M, Corris P, Gaine S, Gibbs JS *et al.* (2009) Guidelines for the diagnosis and treatment of pulmonary hypertension: the Task Force for the Diagnosis and Treatment of Pulmonary Hypertension of the European Society of Cardiology (ESC) and the European Respiratory Society (ERS), endorsed by the International Society of Heart and Lung Transplantation (ISHLT). *Eur Heart J* **30**, 2493–2537.
21 Runo JR & Loyd JE (2003) Primary pulmonary hypertension. *Lancet* **361**, 1533–1544.
22 Chen CS, Weng SC, Tseng PH & Lin HP (2005) Histone acetylation-independent effect of histone deacetylase inhibitors on Akt through the reshuffling of protein phosphatase 1 complexes. *J Biol Chem* **280**, 38879–38887.
23 Thiagalingam S, Cheng KH, Lee HJ, Mineva N, Thiagalingam A & Ponte JF (2003) Histone deacetylases: unique players in shaping the epigenetic histone code. *Ann N Y Acad Sci* **983**, 84–100.
24 Glozak MA, Sengupta N, Zhang X & Seto E (2005) Acetylation and deacetylation of non-histone proteins. *Gene* **363**, 15–23.
25 Yoo CB & Jones PA (2006) Epigenetic therapy of cancer: past, present and future. *Nat Rev Drug Discov* **5**, 37–50.
26 Yang XJ & Seto E (2008) Lysine acetylation: codified crosstalk with other posttranslational modifications. *Mol Cell* **31**, 449–461.
27 Singh BN, Zhang G, Hwa YL, Li J, Dowdy SC & Jiang SW (2010) Nonhistone protein acetylation as cancer therapy targets. *Expert Rev Anticancer Ther* **10**, 935–954.
28 Shimoda LA, Sylvester JT & Sham JS (2000) Mobilization of intracellular Ca(2+) by endothelin-1 in rat intrapulmonary arterial smooth muscle cells. *Am J Physiol Lung Cell Mol Physiol* **278**, L157–164.
29 Young FM, Phungtamdet W & Sanderson BJ (2005) Modification of MTT assay conditions to examine the cytotoxic effects of amitraz on the human lymphoblastoid cell line, WIL2NS. *Toxicol In Vitro* **19**, 1051–1059.
30 Fimognari C, Nüsse M & Hrelia P (1999) Flow cytometric analysis of genetic damage, effect on cell cycle progression, and apoptosis by thiophanate-methyl in human lymphocytes. *Environ Mol Mutagen* **33**, 173–176.
31 Müller KM, Tveteraas IH, Aasrum M, Ødegård J, Dawood M, Dajani O, Christoffersen T & Sandnes DL (2011) Role of protein kinase C and epidermal growth factor receptor signalling in growth stimulation by neurotensin in colon carcinoma cells. *BMC Cancer* **11**, 421.
32 Pfaffl MW, Horgan GW & Dempfle L (2002) Relative expression software tool (REST) for group-wise comparison and statistical analysis of relative expression results in real-time PCR. *Nucleic Acids Res* **30**, e36.

33 Lionetti V, Cantoni S, Cavallini C, Bianchi F, Valente S, Frascari I, Olivi E, Aquaro GD, Bonavita F, Scarlata I *et al*. (2010) Hyaluronan mixed esters of butyric and retinoic acid affording myocardial survival and repair without stem cell transplantation. *J Biol Chem* **285**, 9949–9961.

34 Montanaro L, Govoni M, Orrico C, Treré D & Derenzini M (2011) Location of rRNA transcription to the nucleolar components: disappearance of the fibrillar centers in nucleoli of regenerating rat hepatocytes. *Cell Struct Funct* **36**, 49–56.